Research Square

Preprints are preliminary reports that have not undergone peer review.
They should not be considered conclusive, used to inform clinical practice,
or referenced by the media as validated information.

Quantifying Snowmelt Contribution to Streamflow Using Ensemble Machine Learning and Remote Sensing

Maryam Irani
University of Tehran
Jila Dehghani
University of Guilan
Fatemeh Ghanbari Talouki
Tarbiat Modares University
Mohammad Roohi
mohammad-roohi@stu.scu.ac.ir

Shahid Chamran University of Ahvaz

Research Article

Keywords: Snowmelt contribution, Snow cover estimation, SWE, Random Forest, Remote Sensing, GEE

Posted Date: March 26th, 2026

DOI: https://doi.org/10.21203/rs.3.rs-8440293/v1

License: This work is licensed under a Creative Commons Attribution 4.0 International License.
Read Full License

Additional Declarations: No competing interests reported.

Quantifying Snowmelt Contribution to Streamflow Using Ensemble Machine Learning and Remote Sensing

Nomenclature

EL	Ensemble Learning
FLDAS	Famine Early Warning Systems Network Land Data Assimilation System
GEE	Google Earth Engine
GIS	Geographic Information System
MAE	Mean Absolute Error
ML	Machine Learning
MODIS	Moderate Resolution Imaging Spectroradiometer
MSE	Mean Squared Error
RF	Random Forrest
RMSE	Root Mean Squared Error
SWE	Snow Water Equivalent

Abstract

Snowmelt plays a vital role in sustaining river flows and regulating water resources in mountain ecosystems, particularly under changing climatic conditions. This study aims to quantify the contribution of snowmelt to streamflow by estimating snow cover and snow water equivalent (SWE) in the Greater Caucasus Basin of Azerbaijan. MODIS and FLDAS remote sensing products were analyzed using the Random Forest machine learning algorithm, with data processed on the Google Earth Engine (GEE) platform to improve prediction efficiency and accuracy. Results show that Random Forest significantly enhanced snow cover estimation compared to satellite data alone. MODIS and FLDAS observations revealed peak snow cover in December 2023 (1,310 km²) and maximum SWE in February 2023 (23 kg/m²). Over the longer period 2013–2023, the highest snow cover was recorded in 2016 (5,052 km²), while peak SWE occurred in 2019 (188.7 kg/m²). These findings indicate a weakening role of snow in regional runoff regulation and water supply, driven by declining snowfall and streamflow. The study demonstrates the value of machine learning for snowpack monitoring and highlights the need for long-term simulations and expanded ground-based networks to improve prediction of peak flow events in mountain basins.

Keywords: Snowmelt contribution, Snow cover estimation, SWE, Random Forest, Remote Sensing, GEE

1. Introduction

Snow in mountainous regions is a crucial source of water supply for many catchments, and its importance is amplified under changing climatic conditions (Peker & Sorman 2021). Seasonal snowpack accumulation during cold periods and its ablation in warmer seasons serve as a link between the cryosphere, climate system, surface energy, and water balance. Snowpack contributes substantial freshwater to surface and groundwater reservoirs, supporting agricultural irrigation, hydropower generation, eco-hydrological services, and urban economic activities (Li et al. 2017; Huning & Aghakouchak 2018; Li et al. 2021; Roohi et al. 2023; Shokory et al. 2023; Ives & Price 2023). It also regulates inter-annual and intra-annual streamflow variations by storing water during dry years or seasons and releasing it during wetter periods (Armstrong et al. 2019). Snowmelt characteristics are thus a key component of hydrological modeling, particularly in high-altitude and arid regions where snowmelt dominates water resources (Han et al. 2019; Irani et al. 2024). However, extensive snowmelt can also trigger floods that damage infrastructure, farmland, and urban areas (Sun et al. 2022).

Accurate monitoring of snow cover and SWE in mountainous regions is difficult due to the sparse distribution of ground-based weather stations, which provide localized measurements but are insufficient for large-scale analysis (Schilling et al. 2024; Komeh et al. 2025). Remote sensing datasets such as MODIS and FLDAS offer valuable alternatives, though they remain constrained by cloud cover and the challenges of accurately estimating SWE over long periods (Schilling et al., 2024). Hydrological models like HEC-HMS have been applied to simulate snowmelt runoff (Dimri et al. 2023; Ranjan & Singh 2022), but their accuracy is highly sensitive to parameters such as the antecedent temperature index, underscoring the need for better data integration. For example, Lin et al. (2022) implemented HEC-HMS in a web-based environment and developed empirical relationships between model parameters and time series characteristics to reduce parameter uncertainty. Similarly, Goodarzi et al. (2023) analyzed snow properties in winter and their effects on spring soil moisture in northwest Iran (2000–2020), establishing a linear relationship between snow characteristics and soil moisture at two depths.

Recent advancements in ML and EL have revolutionized snow cover and SWE prediction (Thapa et al. 2024), with the RF algorithm proving particularly effective due to its ability to handle complex datasets (Yang et al. 2020). The GEE platform enhances this process by enabling efficient processing of large-scale remote sensing data, such as MODIS and Landsat, reducing the time and computational burden (Sangeetham 2024). Despite the growing use of GEE in hydrogeological studies, a comprehensive analysis integrating EL and RF to assess snowmelt contributions to streamflow remains underexplored, particularly in regions with limited prior research. Azizi et al. (2024), used machine learning algorithms to snow cover changes using MODIS and Landsat data. The results of their studies have revealed comparable performance

between full and semi-models, whereas the trimmed model exhibited weaker performance. Yang et al. (2020) used the RF model to estimate snow depth at temporal and spatial scales. Temporally and spatially independent datasets were applied to verify the fitted RF algorithms. Their results suggested that the accuracy of fitted RF algorithms was greatly influenced by auxiliary data, especially the geographic location.

Despite the growing use of GEE in hydrological studies, few investigations have quantitatively assessed snowmelt contribution to streamflow by combining MODIS and FLDAS products with ensemble machine-learning approaches. In this study, we estimate key snow parameters — daily snow cover, mean monthly snow cover, and SWE — from Terra/Aqua MODIS and FLDAS datasets within the GEE environment. We apply the Random Forest algorithm (an ensemble of decision trees) to improve snow-cover classification and reduce mapping errors. The study objectives are to: (1) generate snow masks and quantify snowmelt, (2) analyze seasonal snow accumulation and the snowfall-to-precipitation ratio, (3) map spatial variability of snow cover, and (4) enhance the accuracy of snow maps using Random Forest. The results are expected to advance understanding of regional snow–hydrological responses to climate change and support water resources management and ecological restoration. To the best of our knowledge, this is the first study to assess SWE and quantify snowmelt contribution to streamflow on the southern slopes of the Greater Caucasus (Azerbaijan) using MODIS/FLDAS processed in GEE together with a Random Forest–based approach.

2. Material and Methods

This section presents the datasets and methodological framework used to quantify the contribution of snowmelt to streamflow. The workflow integrates satellite-based remote sensing products (MODIS and FLDAS) with the RF machine learning algorithm, implemented on the GEE platform. The methodological steps include: (i) data collection and preprocessing, (ii) generation of snow cover and SWE maps, (iii) RF model training and validation, and (iv) evaluation of snowmelt contribution to streamflow. A schematic flowchart summarizing the overall research framework is provided in Figure 1.

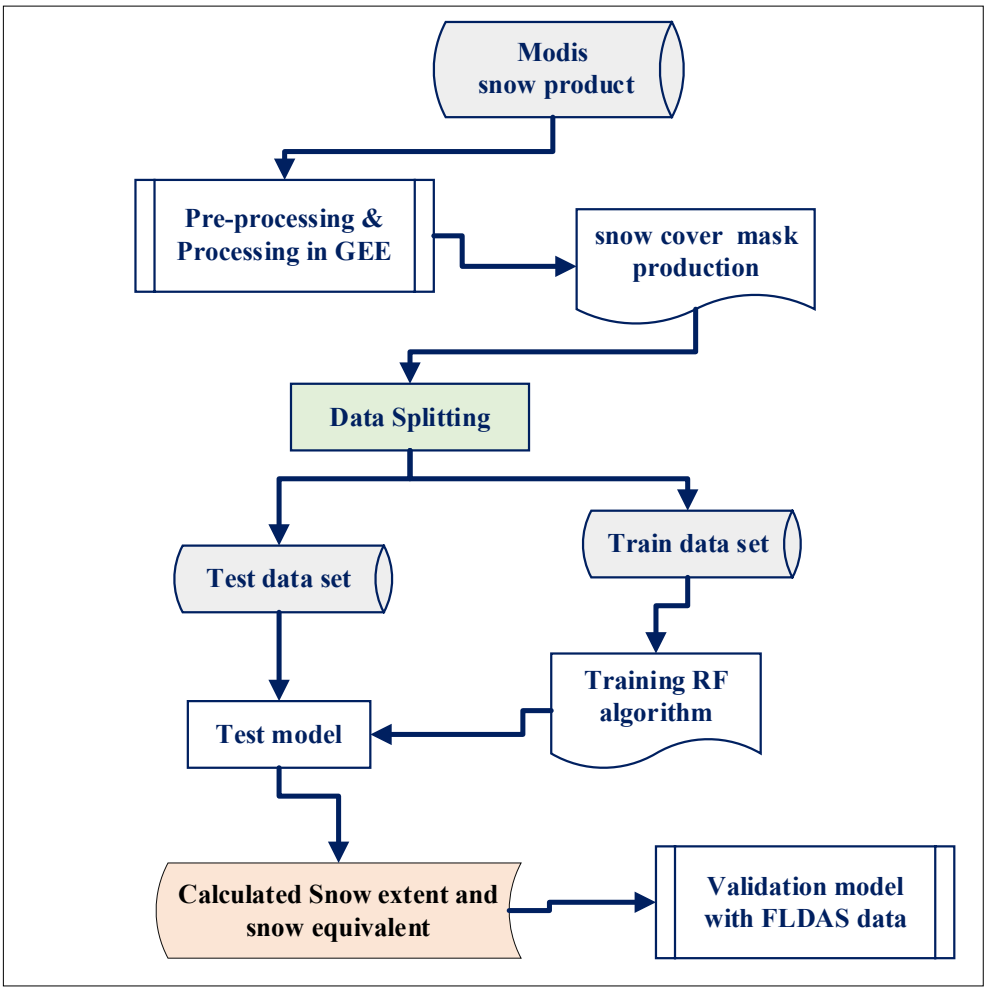


Figure 1 Overall procedure and the conceptual flowchart of the study

92

93 **2.1 Study Area**

94 The Caucasus region is located between the Black Sea and the Caspian Sea. The Greater Caucasus Range
95 is located between the longitude 46° 30′–47° 55′ and the latitude 40° 42′–41° 55′. One of the most important
96 resources offered by the Caucasus Mountains is its water resources, which are stored mainly in glaciers and
97 snow. Meltwater is an important source of several major rivers in the Caucasus region. The Kura River
98 originates from the heights of the Southern Slopes of The Greater Caucasus Range, passes through
99 Azerbaijan, and goes to the Caspian Sea. The catchment basin is in a mountainous area with steep slopes,
100 60% of which includes very steep slopes, the highest point of which is about 4230 m, and the lowest point
101 in the main outlet (Caspian Sea Coastline) is about 200 m. The average annual precipitation of the area is
102 about 700-800 mm. The location of the study area is presented in Figure 2.

The Greater Caucasus is essential for the water supply of the Southern Caucasus countries. In these mountains, the glacier area has decreased from 1674.9±70.4 km2 in 1960 to 1193.2±54.0 km2 in 2014 (Tielidze & Wheate 2018). Average temperature increase has been observed at almost all-weather stations, except for the high mountain station in Terksol (Tashilova et al. 2016). Yearly precipitation varies from the east to the west with 400-600 mm to 600-800 mm in the western part of the plains (van Esch 2019). In the mountains, the precipitation is 800-1300 mm, according to Rets et al. (2018), who studied runoff trends in the Northern Caucasus and gave an overview of the different studies concerning precipitation patterns. The predictions on runoff shortly under the changing climate predict higher runoff during spring due to earlier and faster melting of glaciers and a decrease in summer runoff (Muelchi et al. 2021). Snow cover and glacier development studies are abundant for the Greater/Northern Caucasus; however, it is necessary to study the snow cover and snowmelt in the southern slopes of the greater Caucasus range located in Azerbaijan, which is the focus of this study.

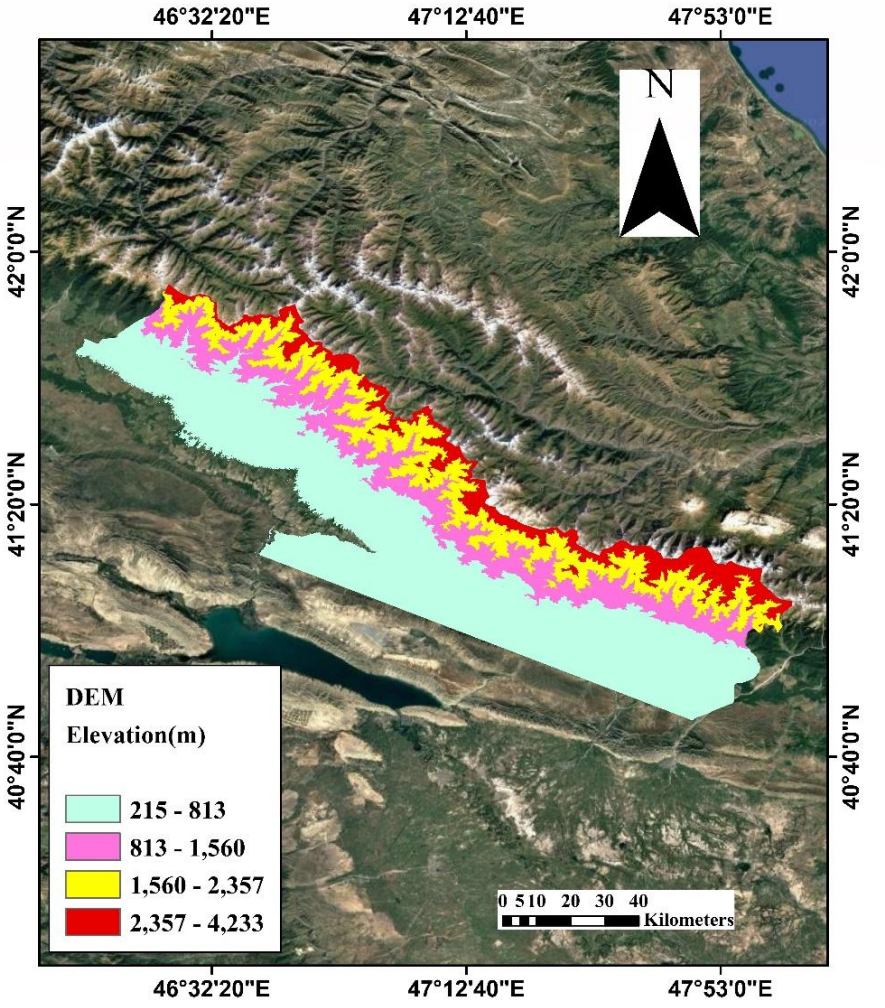


Figure 2 Map of the Study Area: Southern Slopes of the Greater Caucasus Range, Azerbaijan

2.2 Data and Sources

Satellite-based datasets were employed to estimate snow cover and SWE across the study area for the period 2013–2023. The Moderate Resolution Imaging Spectroradiometer (MODIS) onboard the Terra and Aqua satellites was used as the primary source for snow cover mapping. Daily snow cover products (MOD10A1 and MYD10A1) with a spatial resolution of 500 m were extracted to capture spatial and temporal variability in snow dynamics. MODIS has been widely applied in snow-related studies due to its high temporal resolution and global coverage, making it a valuable dataset for monitoring seasonal snowpack and long-term snow trends (Aghashariatmadari et al. 2022; Roohi et al. 2023).

To complement snow cover information, the FLDAS was used to estimate SWE. FLDAS provides gridded data with a spatial resolution of 0.1° (~10 km) and daily temporal resolution, offering consistent estimates of hydrological variables over extended time periods (McNally et al. 2021). The combination of MODIS and FLDAS allows for improved evaluation of both snow cover extent and SWE variability, providing a more comprehensive picture of snowmelt contributions to streamflow. The technical specifications of both datasets are summarized in Table 1. To complement snow cover information, the FLDAS was used to estimate SWE. FLDAS provides gridded data with a spatial resolution of 0.1° (~10 km) and daily temporal resolution, offering consistent estimates of hydrological variables over extended time periods. The combination of MODIS and FLDAS allows for improved evaluation of both snow cover extent and SWE variability, providing a more comprehensive picture of snowmelt contributions to streamflow. The technical specifications of both datasets are summarized in Table 1.

Table 1 Technical specifications of the MODIS and FLDAS datasets used in this study

Satellite/Sensor	Specifications	Data and Products	Applications
Terra (MODIS)	- Launch: December 18, 1999 - Orbit: Polar - Revisit Time: Once per day	36 spectral bands - Data on land surface temperature, vegetation indices, surface moisture, and rainfall	- Natural hazard assessment - Monitoring environmental and climate changes - Water resource management
Aqua (MODIS)	- Orbit: Polar - Revisit Time: Twice per day	- 36 spectral bands - Data on ocean surface, clouds, precipitation, and water vapor	- Monitoring oceans and atmosphere - Weather forecasting - Drought assessment

MODIS (Sensor)	- 36 spectral bands (0.4 to 14.4 micrometers) - Spatial resolution: 250 meters to 1 kilometer	- Products: Vegetation indices, land and water surface temperature, soil moisture indices	- Flood and drought prediction - Climate and environmental change assessment
FLDAS	- Land data assimilation model - Integration of ground and satellite data	- Products: Soil moisture, precipitation, runoff, evapotranspiration	- Drought monitoring - Water and agricultural resource management

2.3 Snow Cover Estimation from MODIS Data

To derive snow cover information, we employed the GEE cloud-based platform, which integrates large geospatial datasets with a functional API for efficient processing. While MODIS data are openly available, downloading the required images separately would be time-consuming and result in several hundred gigabytes of data. Using GEE allowed us to access MODIS archives, perform preprocessing, and extract snow parameters directly online, significantly reducing storage requirements and processing time (Shelestov et al. 2017).

The GEE system facilitates rapid and efficient processing of satellite imagery through its extensive library of free satellite data. To calculate the average monthly snow cover in the study area, MODIS sensor data from the Terra and Aqua satellites were used within the GEE platform. Specifically, the MOD10A1 V6 Snow Cover Daily Global 500m product was employed. This dataset includes snow cover, snow albedo, fractional snow cover, and quality assessment (QA) data. The snow cover data are derived using a snow mapping algorithm based on the Normalized Difference Snow Index (NDSI) and other criteria tests (Hall et al., 2016).

The MODIS sensor captures a wide range of information across 36 spectral bands in the 0.4–14.5 μm range. It provides spatial resolutions of 250 m for two spectral bands, 500 m for five spectral bands, and 1000 m for the remaining 29 bands (Angal et al. 2020). Detailed metadata and band descriptions for MODIS data are available in the GEE catalog:

(https://developers.google.com/earth-engine/datasets/catalog/MODIS_061_MOD10A1#bands).

For this research, the NDSI snow cover and NDSI snow cover class datasets were extracted from the MOD10A1 product using GEE. The NDSI is calculated using Equation 1:

$$NDSI = \frac{band\ 4 - band\ 6}{band\ 4 + band\ 6} \quad (1)$$

MODIS sensors capture data in 36 spectral bands (0.4–14.5 μm) with spatial resolutions of 250 m (2 bands), 500 m (5 bands), and 1,000 m (29 bands) (Angal et al. 2020). The Terra and Aqua satellites together provide near-daily global coverage, which is especially valuable for monitoring snow dynamics in mountainous regions. In the study area, snow cover is mainly concentrated in the northern high-altitude zones, with elevations reaching up to 4,233 m (Fig. 2).

2.4 Estimation of SWE with FLDAS Data

The SWE was estimated using the FLDAS within the GEE platform. FLDAS was developed to support food security and hydrological assessments in data-scarce regions (McNally et al. 2021). The dataset integrates satellite and reanalysis inputs, including MERRA-2 meteorological data and CHIRPS precipitation (Funk et al. 2015), and is based on the Noah land surface model version 3.6.1. FLDAS provides a suite of climate and hydrological variables such as soil moisture, evapotranspiration, soil temperature, precipitation, and SWE at a spatial resolution of 0.1° (~10 km) and daily temporal resolution.

In this study, SWE was calculated directly within the GEE environment by accessing the FLDAS NOAH 3.6.1 daily product. Time series were generated for the 2013–2023 period, and spatial averages were derived for the study basin. Monthly and annual aggregates were then computed to analyze seasonal snow accumulation and melting trends. Processing within GEE minimized data handling requirements and allowed efficient extraction of SWE maps and statistics at both temporal and spatial scales.

SWE estimates from FLDAS are widely used for evaluating snowpack dynamics during accumulation and melt seasons, which are critical inputs for hydrological modeling (Ougahi & Rowan 2024). The accuracy and technical specifications of FLDAS products are documented by NASA (https://ldas.gsfc.nasa.gov/fldas) and through the GEE data catalog:

(https://developers.google.com/earth-engine/datasets/catalog/NASA_FLDAS_NOAH01_C_GL_M_V001).

2.5 ML Algorithm for Snow Cover Estimation

Machine learning was applied in this study to improve the estimation of snow cover extent. Among various ensemble approaches, the RF algorithm was selected due to its robustness in handling nonlinear relationships, resistance to overfitting, and ability to process large geospatial datasets efficiently (Roohi et al. 2025). In this research, RF was implemented within the GEE environment to classify snow and non-snow areas based on MODIS imagery. This section outlines the principles of the RF algorithm and its application for snow cover mapping and validation.

2.5.1 Random Forest (RF)

RF is an ensemble learning method that addresses both classification and regression tasks by aggregating the outputs of multiple decision trees (Roohi et al. 2024; Jin et al. 2024). Each tree is trained on a randomly selected subset of the dataset and predictor variables, and the final prediction is obtained by averaging the outputs of all trees (Roohi et al. 2025). This approach reduces overfitting and improves predictive performance compared to a single decision tree.

In hydrology and cryosphere studies, RF has been widely adopted due to its computational efficiency, robustness to noise, and ability to capture nonlinear relationships in large geospatial datasets (Schoppa et al. 2020). In this study, RF was applied specifically to estimate snow cover from MODIS imagery within the Google Earth Engine environment. The model was configured with 100 decision trees, and the MSE was used as the cost function for evaluating prediction performance.

For regression-type applications, the prediction of a RF can be expressed as (Servati et al. 2014):

$$RF(x) = \frac{1}{K}\sum_{K=1}^{K} Tree_k\,(x) \tag{2}$$

where $RF(x)$ is the Random Forest prediction for the input vector x. K is the number of the trees in the forest. $Tree_K(x)$ is the prediction of the k^{th}decision tree for the input vector x.

In this study, snow cover estimation using the RF algorithm followed a multi-step procedure. First, MODIS daily snow cover images were preprocessed in GEE to generate input features, including the NDSI and ancillary spectral bands. These data were combined with reference snow maps to create training and validation samples. The RF model was then trained on randomly selected subsets of the dataset, with each decision tree learning patterns to distinguish snow from non-snow pixels. After training, the ensemble of 100 decision trees was used to classify snow cover across the study area. Model outputs were validated against independent samples, and statistical performance metrics such as RMSE and MAE were calculated to assess prediction accuracy. This workflow ensured that snow cover maps were derived consistently and efficiently over the 2013–2023 period.

2.5.2 Validation of the RF Model

Model validation assesses how well the trained RF generalizes to unseen data and quantifies the reliability of snow-cover predictions. In this study, the available labeled samples were split into a training set (70%) and an independent testing set (30%). Hyperparameters (e.g., number of trees, maximum depth, minimum samples per leaf) were tuned using k-fold cross-validation (k = 5) on the training subset to avoid overfitting

and to select robust model settings. The final RF model (K = 100 trees) was then evaluated on the held-out test set.

Because the RF model was applied here to estimate snow cover area (km²) and basin-scale SWE (kg m⁻²), model performance was evaluated using continuous error metrics. Specifically, MSE, RMSE, and MAE were calculated to quantify the differences between observed and predicted values at the catchment scale (Deschamps-Berger et al., 2020; Keuris et al. 2023).

The primary metrics used in this study are defined as follows:

$$MSE = (1/n) * \Sigma (y_i - \hat{y}_i)^2 \quad (3)$$

$$RMSE = \sqrt{[(1/n) * \Sigma (y_i - \hat{y}_i)^2]} \quad (4)$$

$$MAE = (1/n) * \Sigma |y_i - \hat{y}_i| \quad (5)$$

where N represents the number of samples in the dataset, Ii is the actual value of the target variable for the $_Ii$ sample, and $_Ii$ hat is the predicted value of the target variable for the $_Ii$ sample. (Ii) ˆ is the estimated flow for sample *i*, *Ii* is the volume of the outflow of a given station, *I* is the average outlet flow of the station. These metrics provide measures of the model's error magnitude, with lower MSE, RMSE and MAE values indicating better accuracy. However, unlike MSE, RMSE, MAE does not account for the direction of the errors, which might be necessary in specific applications (Wang & Oppelt 2023).

3. Results and Discussion

3.1 Snow Cover Variability Derived from MODIS

Snow cover datasets were analyzed from January 2013 to December 2023 using the MODIS MOD10A1 daily product within the GEE environment. Although MODIS data are available from 2000 to the present, this study focused on a consistent 11-year period to align with FLDAS availability and ensure robust temporal comparison. The average monthly snow cover area for 2023 is presented in Table 2, while annual averages for 2013–2023 are summarized in Table 3. Figure 3 illustrates the mean monthly snow cover dynamics across the study area.

The results indicate that snow cover in 2023 peaked during winter, with the largest extent recorded in December (1,310 km²), followed by gradual ablation as temperatures increased in spring. During the summer months (July–August), snow cover was nearly absent, with a minimum of only ~1 km². Long-term statistics (2013–2023) reveal strong seasonal variability: the maximum monthly snow cover reached 1,759 km² in February, while the minimum was close to zero in July and August. On average, snow cover ranged

242 from 3 km² in August to 734 km² in January–February. These results highlight the pronounced seasonality
243 of snow dynamics and their sensitivity to interannual climatic variability.

244 Annual trends (Table 3) further emphasize these variations. The largest annual snow cover was recorded in
245 2016 (5,052 km²), whereas 2018 (2,142 km²) and 2019 (2,143 km²) exhibited the lowest values. The spatial
246 distribution of snow cover indicates that accumulation is concentrated in the upstream high-altitude zones
247 of the basin, particularly in the northwest, where elevations exceed 4,000 m. Such variability is primarily
248 attributed to changes in precipitation patterns and rising winter temperatures associated with regional
249 climate change.

Tabel 2 Average monthly for one-year (2023) and minimum, maximum and average monthly for long term (2013 -2023) values of snow cover and SWE.

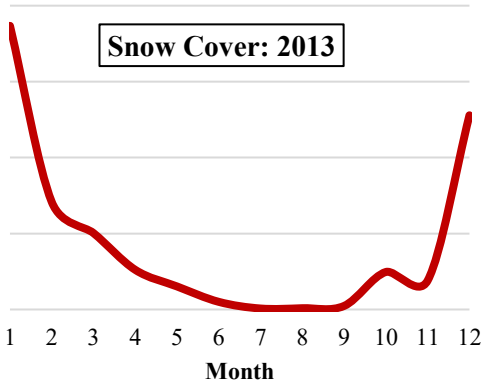
Month	Snow Cover (2023) (km^2)	Minimum Snow Cover (2013-2023) (km^2)	Average Snow Cover (2013-2023) (km^2)	Maximum Snow Cover (2013-2023) (km^2)	Snow Water Equivalent (2023) (kg/m^2)	Minimum Snow Water Equivalent (2013-2023) (kg/m^2)	Average Snow Water Equivalent (2013-2023) (kg/m^2)	Maximum Snow Water Equivalent (2013-2023) (kg/m^2)
January	484	297	733	1,372	16.3	7.2	15.8	38.5
February	273	273	734	1,759	23	8.5	19.4	51.2
March	82	82	255	409	12.1	5.4	16.4	44.6
April	56	56	181	365	5.2	3.4	9.3	32.4
May	27	27	72	107	1.5	0.1	2.2	7.8
June	7	7	23	39	0	0	0	0.1
July	1	0	4	11	0	0	0	0
August	1	0	3	11	0	0	0	0.1
September	8	1	7	16	0	0	0	0.1
October	21	1	89	234	1.5	0.1	1.9	5.8
November	151	115	264	568	2.9	1.1	4.9	12.4
December	1310	293	640	1,310	10.3	6.3	10.5	20.1

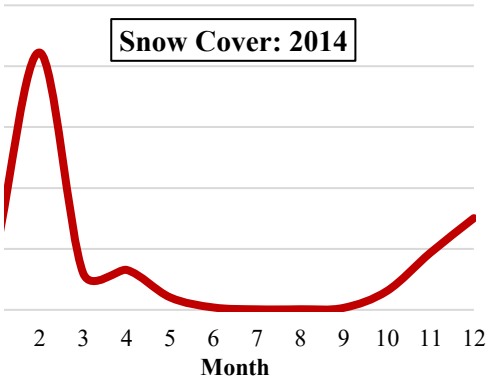
250

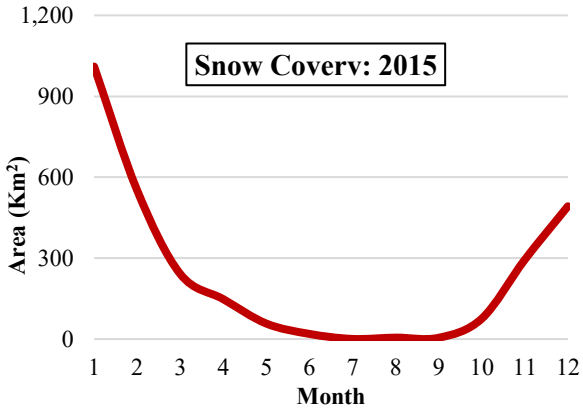
Table 3 Total annual average area of snow cover and SWE from 2013 to 2023

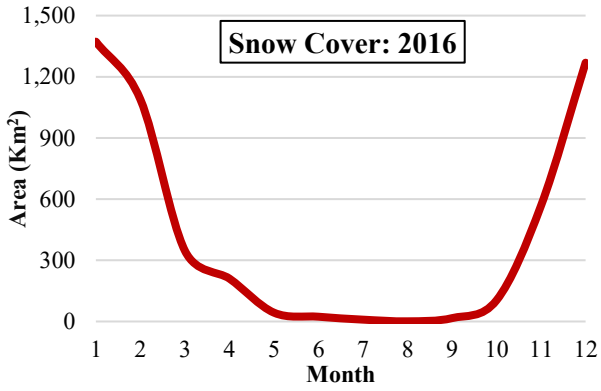
Year	2013	2014	2015	2016	2017	2018	2019	2020	2021	2022	2023
Snow Cover (km^2)	3177	2856	2899	5052	4423	2142	2143	2948	2583	2412	2419
Snow Water Equivalent (kg/m^2)	89.6	44.2	66.8	78.9	72.4	85.7	188.7	56.8	73.3	56.1	72.8

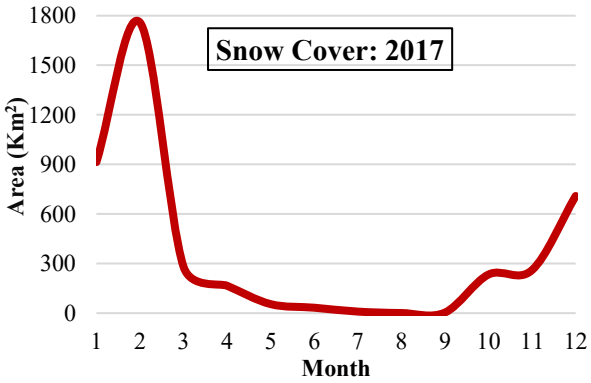
251

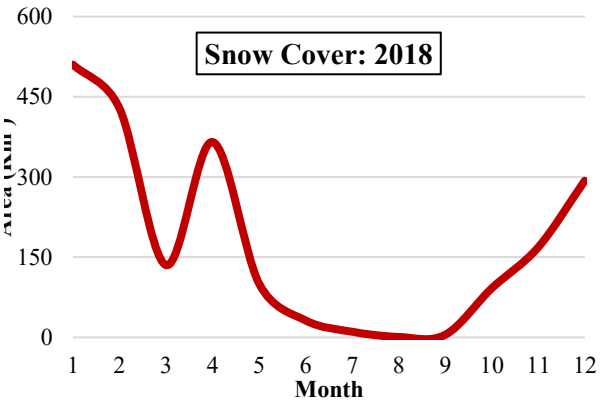

Snow Cover: 2013
1 2 3 4 5 6 7 8 9 10 11 12
Month


Snow Cover: 2014
2 3 4 5 6 7 8 9 10 11 12
Month


Snow Coverv: 2015
1,200
900
600
300
0
Area (Km²)
1 2 3 4 5 6 7 8 9 10 11 12
Month


Snow Cover: 2016
1,500
1,200
900
600
300
0
Area (Km²)
1 2 3 4 5 6 7 8 9 10 11 12
Month


Snow Cover: 2017
1800
1500
1200
900
600
300
0
Area (Km²)
1 2 3 4 5 6 7 8 9 10 11 12
Month


Snow Cover: 2018
600
450
300
150
0
1 2 3 4 5 6 7 8 9 10 11 12
Month

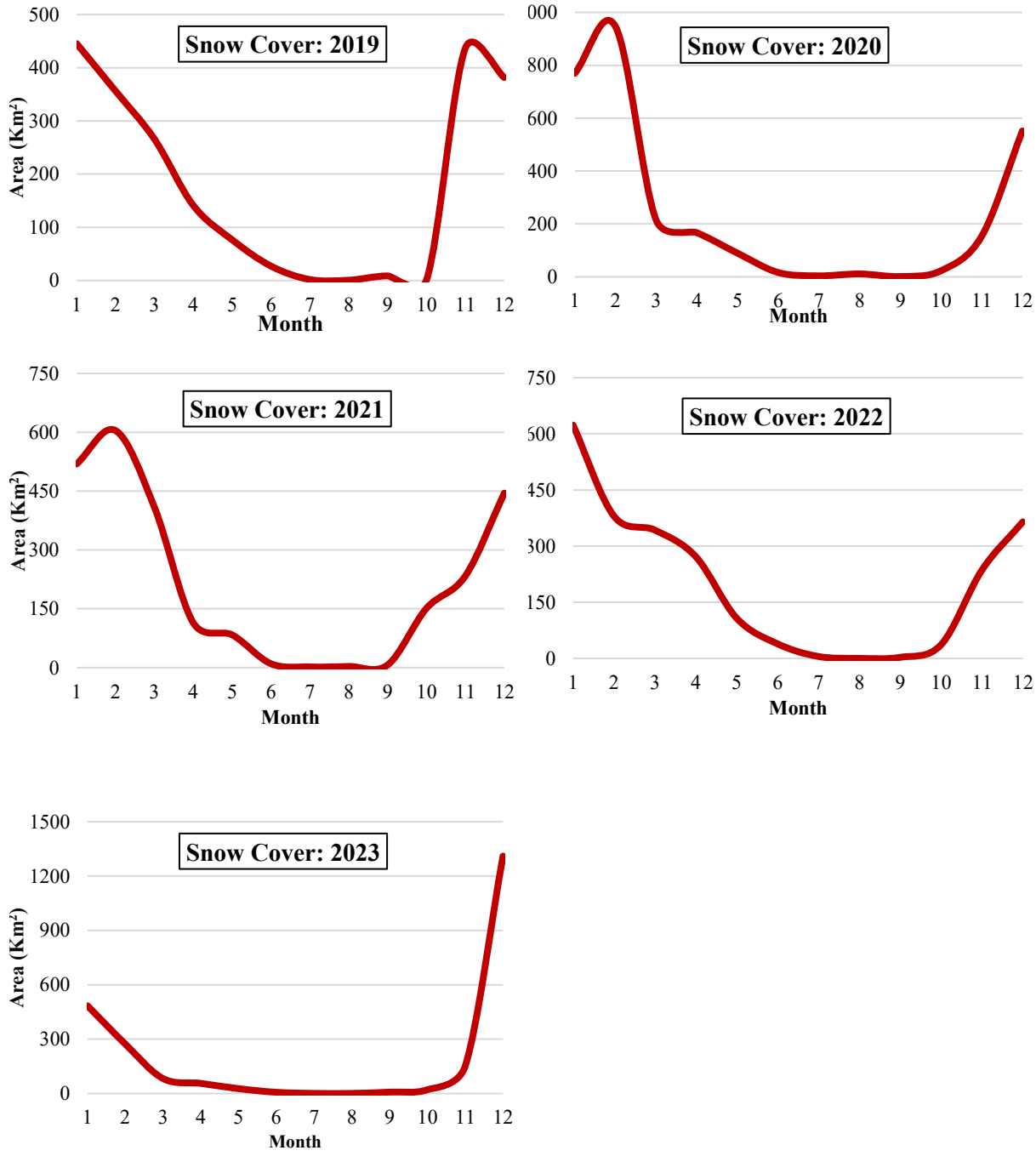


Figure 3 Monthly average snow cover area for each year from 2013 to 2023

252

253 The strong seasonal cycle in snow cover observed in this study is consistent with the climatic characteristics
254 of high-mountain basins, where snow accumulates during winter and gradually melts in spring. The sharp
255 decline in summer snow extent, with values approaching zero, reflects the dominance of high temperatures

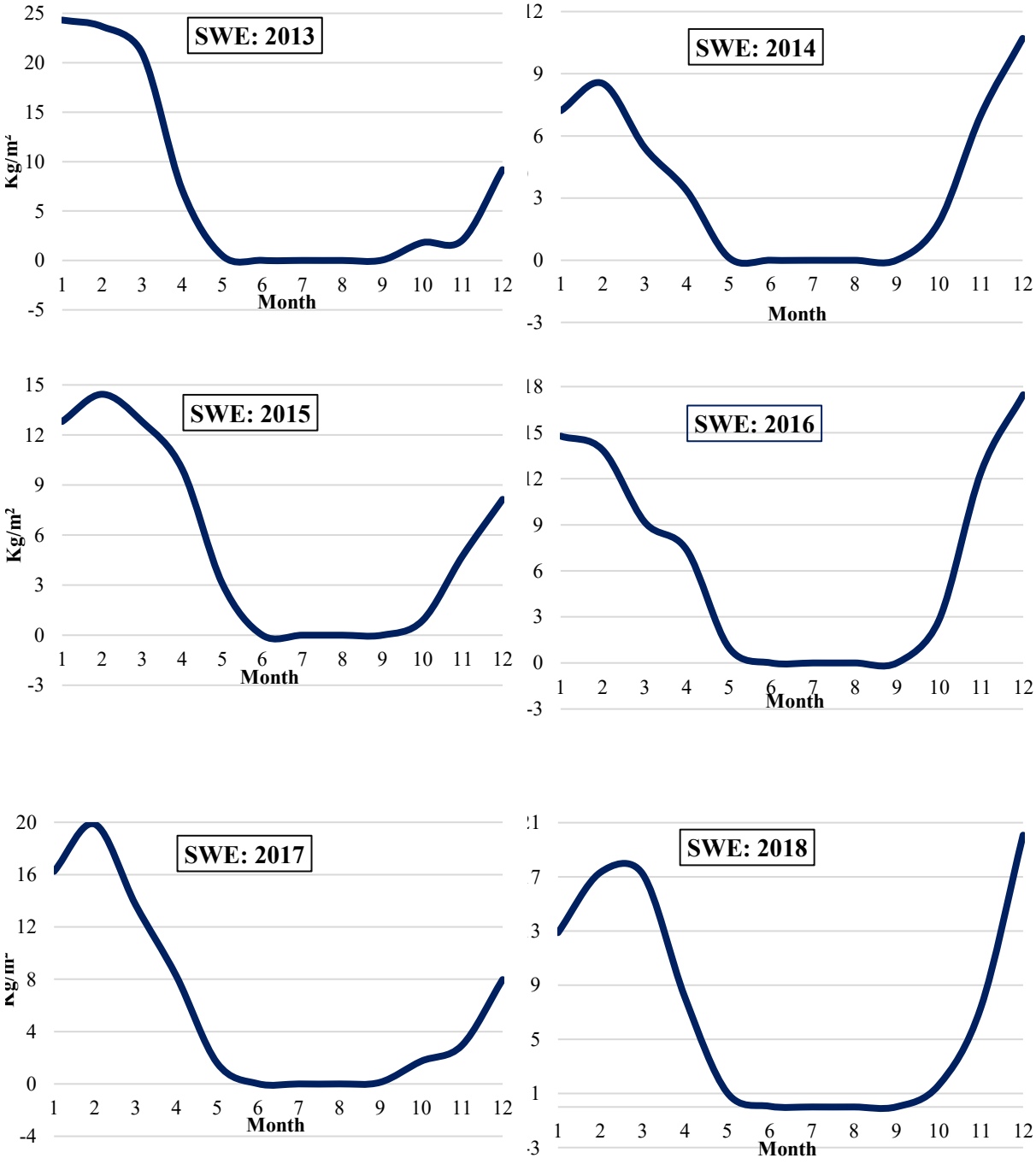
in the ablation process. Interannual variability, such as the exceptionally high snow cover in 2016 and low values in 2018–2019, can be attributed to fluctuations in winter precipitation and rising winter temperatures linked to climate variability and change. Such changes are in line with broader trends reported for mountain regions, where snowpack is becoming increasingly sensitive to warming winters.

Our findings are comparable to previous studies in similar mountain environments. For instance, Roohi et al. (2023) and Shokory et al. (2023) also documented declining snow cover trends in Central Asian and Himalayan catchments, respectively, emphasizing the influence of warming temperatures on seasonal snow dynamics. Similarly, Armstrong et al. (2019) highlighted the regulatory role of snowpack in streamflow, which is weakening due to reduced snow accumulation. The results in the Greater Caucasus thus align with global evidence that climate change is reshaping the temporal and spatial distribution of snow.

From a water resources perspective, these changes in snow cover have important implications. Reduced snow accumulation at high altitudes may lead to diminished spring runoff, which directly affects irrigation supply, hydropower generation, and ecosystem services. The observed variability also suggests greater uncertainty in seasonal water availability, complicating water management and flood forecasting. Therefore, continuous monitoring of snow dynamics using remote sensing and machine learning approaches, as demonstrated in this study, is essential for improving adaptation strategies in snow-dependent basins.

3.2 SWE Variability Derived from FLDAS

SWE data were analyzed for the period January 2013 to December 2023 using the FLDAS NOAH 3.6.1 daily product accessed via the GEE platform. Although FLDAS is available from 1982 onward, the 2013–2023 window was selected to match the MODIS analysis and to ensure consistent temporal coverage with other datasets. The average monthly SWE for 2023 is reported in Table 2, annual SWE statistics for 2013–2023 are given in Table 3, and monthly SWE patterns are illustrated in Figure 4.


SWE: 2013
Kg/m²
Month
SWE: 2014
Month
SWE: 2015
Kg/m²
Month
SWE: 2016
Month
SWE: 2017
Month
SWE: 2018
Month

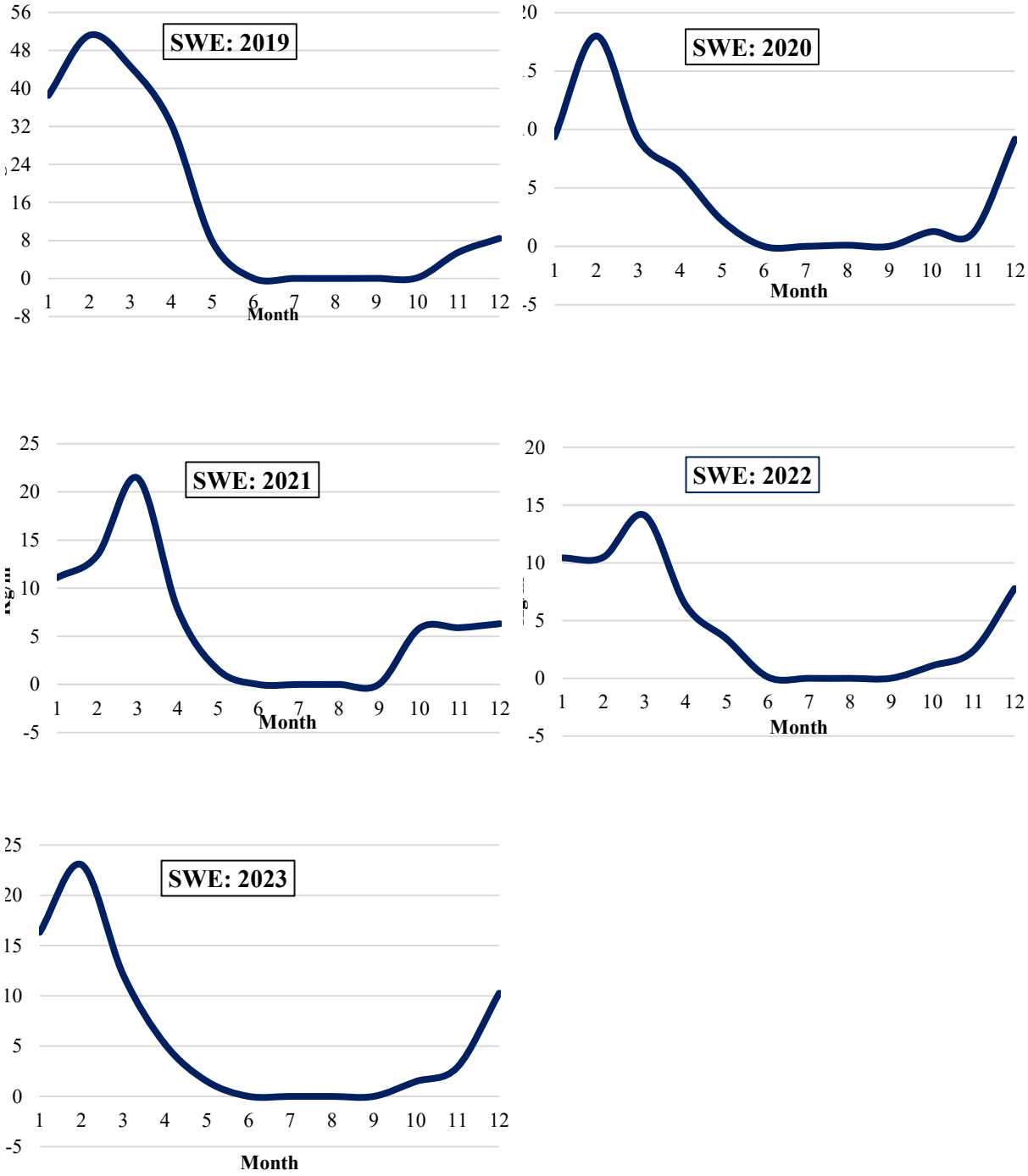


Figure.4 Average monthly SWE for each year from 2013 to 2023.

280

281 For 2023, SWE peaked in February with a value of 23.0 kg m^{-2} and decreased to near-zero values during
282 the summer months (June–September). Across the full 2013–2023 period, monthly SWE values generally

ranged from 0 kg m^{-2} in summer to markedly higher values in winter, with typical February monthly maxima varying roughly between ~8.5 and ~51.2 kg m^{-2} depending on the year. The long-term (2013–2023) mean February SWE was 19.4 kg m^{-2}, highlighting substantial interannual variability in winter snow storage.

At annual scale, the largest mean basin SWE was observed in 2019 (188.7 kg m^{-2}), while 2014 showed the lowest annual mean SWE (44.2 kg m^{-2}) over the study period. These interannual fluctuations reflect variability in winter precipitation totals and temperature-driven partitioning between rain and snow. It should be noted that FLDAS's coarse spatial resolution (~0.1° ≈ 10 km) can smooth local extremes in high-relief terrain; therefore, comparisons with in-situ snow observations (where available) or higher-resolution products are recommended to better constrain uncertainties. Future analysis could also include formal trend tests (e.g., Mann–Kendall) and correlation analysis between annual SWE and streamflow or precipitation to quantitatively link SWE variability to hydrological impacts.

The seasonal cycle of SWE derived from FLDAS clearly reflects the influence of both precipitation and temperature on snowpack accumulation and ablation. Peak values occurring in February correspond to maximum winter snowfall and stable subzero temperatures, while the sharp decline to near-zero SWE during June–September highlights rapid melting in response to elevated summer temperatures. The interannual differences, with exceptionally high SWE in 2019 and notably low values in 2014, likely result from shifts in winter precipitation patterns and warmer-than-average winters, which reduced the proportion of snowfall relative to rainfall.

These findings are consistent with previous studies in other mountain regions. For example, Musselman et al. (2017) and Barnhart et al. (2016) emphasized that warming winters accelerate snowpack depletion, leading to declining SWE trends. Similarly, studies in the Himalayas and Central Asia (Bhat et al. 2025; Gottlieb & Mankin 2024) also reported strong year-to-year fluctuations in SWE linked to variability in precipitation intensity and temperature extremes. The variability observed in the Greater Caucasus Basin therefore aligns with broader global evidence that snowpacks are becoming increasingly sensitive to climate change.

From a hydrological perspective, the observed SWE variability has important implications for regional water security. Reduced SWE storage not only diminishes the potential spring runoff but also disrupts the timing of peak streamflow, complicating water allocation for agriculture, hydropower, and ecological needs. The exceptionally high SWE in 2019 illustrates that occasional years of heavy snowfall can still occur, increasing the risk of snowmelt-driven floods, while years of low SWE (e.g., 2014) can intensify drought conditions. These dual risks underscore the importance of continuous SWE monitoring and

integration of remote sensing products like FLDAS with in-situ data to support adaptive water resource management and flood preparedness strategies in snow-dependent catchments.

3.3 Snow Cover and SWE Estimation Using the RF Model

The RF algorithm was applied to estimate snow cover and SWE using the preprocessed MODIS and FLDAS datasets. Input features were normalized prior to model training, and the dataset was split into training (70%) and testing (30%) subsets to ensure reliable validation. Four snow cover mask images were withheld exclusively for independent model testing.

The RF model demonstrated strong predictive capability, achieving an accuracy of approximately 95% on the training dataset. Comparison of observed and predicted values for snow cover and SWE (Table 4) confirmed that the RF algorithm effectively captured the spatial and temporal variability of snow dynamics. Evaluation metrics further highlighted the model's performance: MSE, RMSE, and MAE were estimated at 268.3 km^2, 16.3 km^2, and 15.1 km^2, respectively, for snow cover, and 5.5 kg m^{-2}, 2.3 kg m^{-2}, and 2.3 kg m^{-2}, respectively, for SWE (Table 5). Figure 5 illustrates examples of predicted snow cover masks compared to observed images during the testing phase, showing a strong visual agreement between the two.

Table 4 Prediction results of RF model for test images

Test mask images	Predicted		Observed	
	Snow Cover (km^2)	SWE (kg/m^2)	Snow Cover (km2)	SWE (kg/m2)
Snow Cover Feb2015	525	12.3	551	14.4
Snow Cover Apr2020	180	9.3	167	6.4
Snow Cover Jan2022	633	12.9	623	10.4
Snow Cover Dec2023	1320	12	1309	10.3

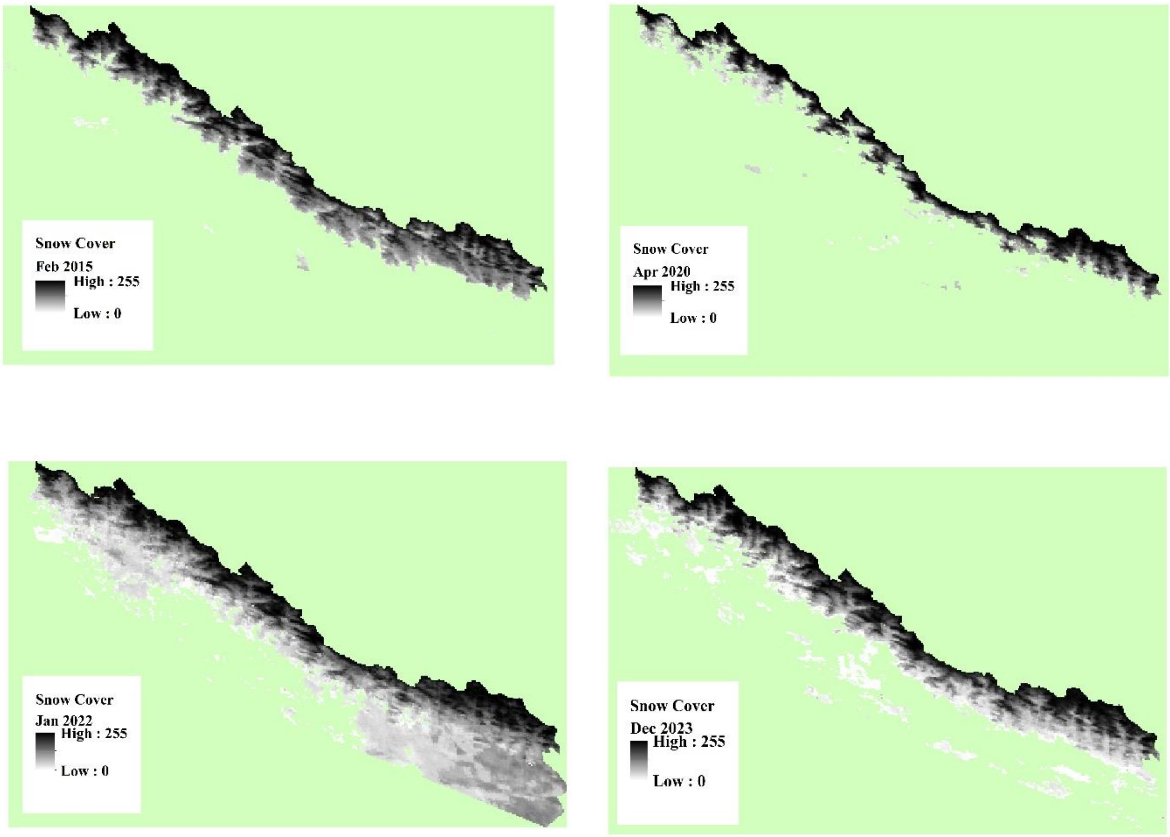


Fig 5. RF-derived snow cover maps used for model testing.

331

Table 5 Performance metrics of the RF model for snow cover area and SWE prediction on the test dataset

Parameter	MSE	RMSE	MAE
Snow Cover (km²)	268.3	16.3	15.1
SWE (kg/m²)	5.5	2.3	2.3

332

333 These results demonstrate that the RF algorithm provides a robust approach for snow cover and SWE
334 estimation in mountainous regions. By integrating multiple predictors, RF effectively captures the nonlinear
335 relationships between climatic drivers and snow processes, outperforming traditional empirical methods.
336 Nevertheless, snow cover and runoff dynamics are strongly influenced by temperature, precipitation, and
337 other climatic variables that can vary considerably from year to year. Extending the simulation period and
338 integrating additional predictor variables, such as topography and land cover, would further improve the
339 accuracy of future predictions. The demonstrated performance of the RF model highlights its potential for

operational snow monitoring and for supporting downstream water resource management, particularly in basins that are highly dependent on snowmelt-driven streamflow.

The high accuracy of the RF model in predicting snow cover and SWE highlights its ability to handle nonlinear relationships and interactions among multiple predictor variables. Unlike traditional regression-based or empirical snow models, RF can effectively integrate diverse inputs such as temperature, precipitation, and remotely sensed indices, thereby reducing uncertainties that arise from parameter sensitivity. The relatively low RMSE and MAE values obtained in this study indicate that RF is a reliable tool for monitoring snow dynamics in data-scarce mountainous basins.

These findings are consistent with previous applications of machine learning in hydrology. Schoppa et al. (2020) and Roohi et al. (2025) reported that RF outperformed other machine learning algorithms in snow and streamflow modeling due to its robustness against overfitting and its efficiency in processing large datasets. Similarly, recent studies in mountainous regions of Iran and Central Asia have confirmed that ensemble methods, particularly RF, provide superior predictive accuracy compared to empirical temperature-index models and conventional hydrological approaches. The outcomes of this study therefore reinforce the growing evidence that machine learning can complement or even replace traditional snow modeling techniques under changing climatic conditions.

From a practical standpoint, the ability of RF to generate accurate snow cover maps and SWE estimates has important implications for regional water resource management. Reliable predictions can improve flood forecasting during peak melt periods and enhance planning for irrigation and hydropower operations in snow-dependent catchments. However, snowpack dynamics are influenced by complex processes, including topography, vegetation, and microclimatic variations, which are not fully captured by current satellite products. Future research should extend the model to longer time series, integrate higher-resolution satellite imagery, and explore hybrid approaches that combine RF with deep learning architectures. Such improvements will help reduce uncertainties and provide more reliable decision-support tools for managing water resources in snow-dominated basins.

4. Conclusion

This study quantified snowmelt contribution to streamflow by combining MODIS (MOD10A1) snow-cover products and FLDAS SWE estimates within the GEE environment for the 2013–2023 period. Snow-cover maps were produced from MODIS and SWE was extracted from FLDAS, while the RF algorithm (an ensemble of decision trees) was applied to improve pixel-level snow/no-snow classification from MODIS imagery. Key empirical results indicate peak monthly snow cover of 1,310 km² (December 2023) and peak monthly SWE of 23.0 kg m^{-2} (February 2023). Over 2013–2023 the largest annual snow cover and SWE

occurred in 2016 (5,052 km²) and 2019 (188.7 kg m⁻²), respectively. Mean basin-scale monthly snow cover varied from ≈3 km² (August) to ≈734 km² (January–February), and mean February SWE was ≈19.4 kg m⁻², demonstrating pronounced seasonal and interannual variability.

The Random Forest approach substantially improved snow-cover estimation compared to uncorrected MODIS products: the model achieved ~95% accuracy on training data, and basin-scale error statistics for the independent test data were RMSE = 16.3 km² and MAE = 15.1 km² for snow cover. Aggregated SWE comparison (from FLDAS) yielded RMSE ≈ 2.3 kg m⁻² and MAE ≈ 2.3 kg m⁻², indicating that the combined MODIS–FLDAS workflow provides consistent estimates of snow storage at basin scale. These performance metrics underscore the value of using an ensemble decision-tree method for robust classification in complex, mountainous terrain.

The observed reductions in snow storage in some years and the large interannual variability have important hydrological implications: a weakening role of snowpack in regulating seasonal runoff may reduce spring water availability for irrigation and hydropower, while episodic heavy snow years continue to pose flood risks during rapid melt. For water managers, improved monitoring based on satellite products and machine-learning classification can support more reliable seasonal forecasts, flood preparedness, and water-allocation planning in snow-dependent catchments. This study has limitations that suggest directions for future work. FLDAS's coarse spatial resolution (~0.1° ≈ 10 km) and MODIS sensitivity to cloud cover can smooth or obscure local extremes in steep terrain; in-situ observations remain scarce in the study basin and would strengthen calibration/validation. We therefore recommend (i) extending the analysis to longer time series and applying trend tests (e.g., Mann–Kendall) to assess significant changes, (ii) integrating higher-resolution optical/sar products (e.g., Sentinel-2, Landsat, Sentinel-1) or downscaled reanalysis for local-scale improvements, (iii) combining RF-based mapping with physically based hydrological models for improved runoff simulation, and (iv) expanding ground monitoring networks to reduce uncertainty. Implementing these steps will enhance the reliability of snowmelt predictions and better inform decision-support systems for water resource management under a changing climate.

In summary, the combined use of MODIS and FLDAS within GEE together with Random Forest classification produces a practical and effective workflow for monitoring snow cover and estimating basin-scale SWE. The approach provides actionable insights for water resources planning, while further gains are achievable by increasing spatial resolution, length of record, and ground-based validation.

Supplementary Information

Supplementary material associated with this article, including additional tables, is available in the online version.

Data Availability Statement

The datasets generated and analyzed during the current study are publicly available on Figshare at:

https://doi.org/10.6084/m9.figshare.30575462

This repository includes processed MODIS-derived snow cover products, FLDAS-derived snow water equivalent (SWE) data, and Random Forest model outputs (including training/testing masks and prediction results) used in this study. Raw satellite data (MODIS MOD10A1 and FLDAS Noah v3.6.1) are accessible via Google Earth Engine. All data are shared for academic and research purposes under a Creative Commons Attribution 4.0 International License (CC BY 4.0). Additional data or code can be obtained from the corresponding author upon reasonable request.

References

Aghashariatmadari Z, Golmohammadian H, Shariatmadari Z, Mohebbi F, Bazrafshan J (2022) Satellite-based monitoring of the algal communities of aras dam reservoir: meteorological dependence analysis and the footprint of COVID-19 pandemic lockdown on the eutrophication status. Int J Environ Res 16(5):70. https://doi.org/10.1007/s41742-022-00447-0

Angal A, Xiong X, Shrestha A (2020) Cross-Calibration of MODIS Reflective Solar Bands with Sentinel 2A/2B MSI Instruments. IEEE Trans Geosci Remote Sens 58(7):5000–5007. https://doi.org/10.1109/TGRS.2020.2971462

Armstrong R, Rittger K, Brodzik M, Racoviteanu A, Barrett A, Khalsa S, Armstrong B (2019) Runoff from Glacier Ice and Seasonal Snow in High Asia: Separating Melt Water Sources in River Flow. Reg Environ Change 19:1249–1261. https://doi.org/10.1007/s10113-018-1429-0

Azizi A, Akhtar F, Kusche J, Tischbein B, Borgemeister C, Oluoch W (2024) Machine Learning-Based Estimation of Fractional Snow Cover in the Hindukush Mountains Using MODIS and Landsat Data. J Hydrol 638:131579. https://doi.org/10.1016/j.jhydrol.2024.131579

Barnhart T, Molotch N, Livneh B, Harpold A, Knowles J, Schneider D (2016) Snowmelt Rate Dictates Streamflow. Geophys Res Lett 43(15):8006–8016. https://doi.org/10.1002/2016GL069690

Bhat A, Dhondiram P, Gupta S, Kanga S, Singh S, Meraj G, Sajan B (2025) Snow Resources and Climatic Variability in Jammu and Kashmir, India. Climate 13(2):28. https://doi.org/10.3390/cli13020028

Deschamps-Berger C, Gascoin S, Berthier E, Deems J, Gutmann E, Dehecq A, Dumont M (2020) Snow Depth Mapping from Stereo Satellite Imagery in Mountainous Terrain: Evaluation Using Airborne Lidar Data. Cryosphere Discuss 2020:1–28. https://doi.org/10.5194/tc-14-2925-2020

Dimri T, Ahmad S, Sharif M (2023) Hydrological Modelling of Bhagirathi River Basin Using HEC-HMS. J Appl Water Eng Res 11(2):249–261. https://doi.org/10.1080/23249676.2022.2099471

Goodarzi M, Sabaghzadeh M, Niazkar M (2023) Evaluation of Winter Snow Properties Effects on Spring Soil Moisture Using Satellite Images in the Northwest of Iran. Acta Geophys 1–13. https://doi.org/10.1007/s11600-023-01177-3

Gottlieb A, Mankin J (2024) Evidence of Human Influence on Northern Hemisphere Snow Loss. Nature 625(7994):293–300. https://doi.org/10.1038/s41586-023-06794-y

Hagg W, Shahgedanova M, Mayer C, Lambrecht A, Popovnin V (2010) A Sensitivity Study for Water Availability in the Northern Caucasus Based on Climate Projections. Glob Planet Change 73(3–4):161–171. https://doi.org/10.1016/j.gloplacha.2010.05.005

Hall D, Salomonson V, Riggs G (2016) MODIS/Terra Snow Cover Daily L3 Global 500m Grid. Version 6. Boulder, Colorado USA: NASA National Snow and Ice Data Center Distributed Active Archive Center. https://doi.org/10.5067/MODIS/MOD10A1.006

Han P, Long D, Han Z, Du M, Dai L, Hao X (2019) Improved Understanding of Snowmelt Runoff from the Headwaters of China's Yangtze River Using Remotely Sensed Snow Products and Hydrological Modeling. Remote Sens Environ 224:44–59. https://doi.org/10.1016/j.rse.2019.01.041

Huning L, AghaKouchak A (2018) Mountain Snowpack Response to Different Levels of Warming. Proc Natl Acad Sci 115(43):10932–10937. https://doi.org/10.1073/pnas.1805953115

Irani M, Salimi M, Talouki F, Roohi M (2024) Assessing the Impacts of Climate Change on the Vulnerability of Coastal Aquifers to the Seawater Intrusion. Discover Civ Eng 1(1):109. https://doi.org/10.1007/s44290-024-00117-4

Ives K, Price M (2023) The Importance of Snowpack as a Water Source for California.

Jin X, Chen X, Gao L, Wu Y, Lu H, Yuan M, Wei F (2024) Fluorescence Analysis of River DOM Spectra Using PARAFAC in Combination with a Self-Organizing Map to Distinguish Organic Matter Sources. Int J Environ Res 18(2):20. https://doi.org/10.1007/s41742-024-00574-w

Keuris L, Hetzenecker M, Nagler T, Mölg N, Schwaizer G (2023) An Adaptive Method for the Estimation of Snow-Covered Fraction with Error Propagation for Applications from Local to Global Scales. Remote Sens 15(5):1231. https://doi.org/10.3390/rs15051231

Komeh Z, Hamzeh S, Memarian H, Attarchi S, Alavipanah S (2025) A Remote Sensing Approach to Spatiotemporal Analysis of Land Surface Temperature in Response to Land Use/Land Cover Change via Cloud Base and Machine Learning Methods, Case Study: Sari Metropolis, Iran. Int J Environ Res 19(3):98. https://doi.org/10.1007/s41742-025-00752-4

Li D, Wrzesien M, Durand M, Adam J, Lettenmaier D (2017) How Much Runoff Originates as Snow in the Western United States, and How Will That Change in the Future? Geophys Res Lett 44(12):6163–6172. https://doi.org/10.1002/2017GL073551

Li S, Liu M, Adam J, Pi H, Su F, Li D, Yao Z (2021) Contribution of Snowmelt Water to the Streamflow over the Three-River Headwater Region, China. Remote Sens 13(8):1585. https://doi.org/10.3390/rs13081585

Lin Q, Lin B, Zhang D, Wu J (2022) Web-Based Prototype System for Flood Simulation and Forecasting Based on the HEC-HMS Model. Environ Modell Softw 158:105541. https://doi.org/10.1016/j.envsoft.2022.105541

McNally A, Jacob J, Arsenault K, Slinski K, Sarmiento D, Hoell A, Verdin J (2021) A Hydrologic Monitoring Dataset for Food and Water Security Applications in Central Asia. Earth Syst Sci Data Discuss 2021:1–32. https://doi.org/10.5194/essd-2021-420

Muelchi R, Rössler O, Schwanbeck J, Weingartner R, Martius O (2021) River Runoff in Switzerland in a Changing Climate–Runoff Regime Changes and Their Time of Emergence. Hydrol Earth Syst Sci 25(6):3071–3086. https://doi.org/10.5194/HESS-25-3071-2021

Musselman K, Clark M, Liu C, Ikeda K, Rasmussen R (2017) Slower Snowmelt in a Warmer World. Nat Clim Chang 7(3):214–219. https://doi.org/10.1038/nclimate3225

Ougahi J, Rowan J (2024) Combining Hydrological Models and Remote Sensing to Characterize Snowpack Dynamics in High Mountains. Remote Sens 16(2):264. https://doi.org/10.3390/rs16020264

Peker I, Sorman A (2021) Application of SWAT Using Snow Data and Detecting Climate Change Impacts in the Mountainous Eastern Regions of Turkey. Water 13(14):1982. https://doi.org/10.3390/w13141982

Ranjan S, Singh V (2022) HEC-HMS Based Rainfall-Runoff Model for Punpun River Basin. Water Pract Technol 17(5):986–1001. https://doi.org/10.2166/wpt.2022.033

Rets E, Dzhamalov R, Kireeva M, Frolova N, Durmanov I, Telegina A, Grigoriev V (2018) Recent Trends of River Runoff in the North Caucasus. Geogr Environ Sustain 11(3):61–70. https://doi.org/10.24057/2071-9388-2018-11-3-61-70

Roohi M, Dehghani J, Irani M, Mina P (2025) A Comprehensive Review of Flood Damage in Mountainous Regions: Challenges, Solutions, and Advanced Management Technologies. Discover Geosci 3(1):59. https://doi.org/10.1007/s44288-025-00145-2

Roohi M, Faeli M, Jamshidi F, Ghasroddashti A (2023) Snow Parameters Modeling Using Remote Sensing Techniques and HEC-HMS Hydrological Modeling—Case Study: Kan Basin. Environ Monit Assess 195(6):684. https://doi.org/10.1007/s10661-023-11326-2

Roohi M, Ghafouri H, Ashrafi S (2024) Developing an Ensemble Machine Learning Approach for Enhancing Flood Damage Assessment. Int J Environ Res 18(5):90. https://doi.org/10.1007/s41742-024-00647-w

Roohi M, Ghafouri H, Ashrafi S (2025) Advancing Flood Disaster Management: Leveraging Deep Learning and Remote Sensing Technologies. Acta Geophys 73(1):557–575. https://doi.org/10.1007/s11600-024-01481-6

Roohi M, Ghafouri H, Ashrafi S, Motagh M, Haghighi M (2025) A Hybrid Approach for Enhanced Flood Prediction and Assessment: Leveraging Physical Models, Deep Learning and Satellite Remote Sensing. Big Earth Data 1–34. https://doi.org/10.1080/20964471.2025.2530850

Sangeetham R (2024) A Review On Google Earth Engine: An Open Access Cloud Analysis Platform For Planetary Scale Satellite Data. In: E3S Web of Conferences, vol. 591, p. 09011. EDP Sciences. https://doi.org/10.1051/e3sconf/202459109011

Schilling S, Dietz A, Kuenzer C (2024) Snow Water Equivalent Monitoring—A Review of Large-Scale Remote Sensing Applications. Remote Sens 16(6):1085. https://doi.org/10.3390/rs16061085

Schoppa L, Disse M, Bachmair S (2020) Evaluating the Performance of Random Forest for Large-Scale Flood Discharge Simulation. J Hydrol 590:125531. https://doi.org/10.1016/j.jhydrol.2020.125531

Servati M, Ghahrodi Tali M, Golkarami A, Njafi E (2014) Geomorphological Thresholds for Gully Erosion in Kchick Watershed, NE Golestan Province. Appl Res Geogr Sci 32:231–249.

Shelestov A, Lavreniuk M, Kussul N, Novikov A, Skakun S (2017) Exploring Google Earth Engine Platform for Big Data Processing: Classification of Multi-Temporal Satellite Imagery for Crop Mapping. Front Earth Sci 17. https://doi.org/10.3389/feart.2017.00017

Shokory J, Schaefli B, Lane S (2023) Water Resources of Afghanistan and Related Hazards Under Rapid Climate Warming: A Review. Hydrol Sci J 68(3):507–525. https://doi.org/10.1080/02626667.2022.2159411

Sun N, Yan H, Wigmosta M, Coleman A, Leung L, Hou Z (2022) Datasets for Characterizing Extreme Events Relevant to Hydrologic Design over the Conterminous United States. Sci Data 9(1):154. https://doi.org/10.1038/s41597-022-01221-9

Tashilova A, Kesheva L, Teunova N, Taubekova Z (2016) Analysis of Temperature Variability in the Mountain Regions of the North Caucasus in 1961–2013. Russ Meteorol Hydrol 41(9):601–609. https://doi.org/10.3103/S1068373916090028

Thapa K, Singh B, Savalkar S, Fern A, Rajagopalan K, Kalyanaraman A (2024) Attention-Based Models for Snow-Water Equivalent Prediction. In: Proceedings of the AAAI Conference on Artificial Intelligence, vol. 38, no. 21, pp. 22969–22975. https://doi.org/10.1609/aaai.v38i21.30337

Tielidze L, Wheate R (2018) The Greater Caucasus Glacier Inventory (Russia, Georgia and Azerbaijan). Cryosphere 12(1):81–94. https://doi.org/10.5194/tc-12-81-2018

Wang M, Oppelt N (2023) Estimating Early Summer Snow Depth on Sea Ice Using a Radiative Transfer Model and Optical Satellite Data. Remote Sens 15(20):5016. https://doi.org/10.3390/rs15205016

Yang J, Jiang L, Luojus K, Pan J, Lemmetyinen J, Takala M, Wu S (2020) Snow Depth Estimation and Historical Data Reconstruction over China Based on a Random Forest Machine Learning Approach. Cryosphere 14(6):1763–1778. https://doi.org/10.5194/tc-14-1763-2020

Statements and Declarations

Funding

The authors declare that no funds, grants, or other support were received during the preparation of this manuscript.

Competing Interests

The authors have no relevant financial or non-financial interests to disclose.

Author Contributions

Maryam Irani contributed to data collection, preprocessing, and analysis, including the extraction of snow cover and snow water equivalent datasets using MODIS and FLDAS products. Jila Dehghani contributed to methodology development, machine learning model implementation, and validation of the Random Forest algorithm. Fatemeh Ghanbari Talouki assisted in data interpretation, visualization of results, and preparation of figures and tables. Mohammad Roohi conceptualized the study, supervised the research, contributed to result interpretation, and reviewed and edited the manuscript. All authors read and approved the final manuscript.

Consent To Participate

All authors whose names appear on the submission (1) made substantial contributions to the conception or design of the work; or the acquisition, analysis, or interpretation of data; or the creation of new software used in the work. (2) drafted the work or revised it critically for important intellectual content. (3) approved the version to be published; and (4) agree to be accountable for all aspects of the work in ensuring that questions related to the accuracy or integrity of any part of the work are appropriately investigated and resolved.

Consent To Publish

All authors listed in the submission agree to the publication of the paper.

Competing interests

The authors declare that they have no known competing financial interests.